Proceedings of IMECE 2000
International Mechanical Engineering Congress & Exposition
November 5-10, 2000, Orlando, Florida, USA

TIME-DEPENDENT CALCULATION OF ACOUSTIC RADIATION FROM FINITE WINGS USING BEM

Trevor H. Wood*
Department of Aerospace and Mechanical Engineering
Boston University
Boston, Massachusetts 02215
Email: twood@bu.edu

Sheryl M. Grace†
Department of Aerospace and Mechanical Engineering
Boston University
Boston, Massachusetts 02215
Email: sgrace@bu.edu

ABSTRACT

The calculation of acoustic radiation from finite wings using a 3D, time-domain Boundary Element Method (BEM) was investigated. Numerical convergence was studied and solutions obtained using an extrapolated convergence method were used to compare to 2D analytical solutions. Frequency-domain lift solutions were found to be accurate to less than 5% using relatively coarse grids ($\Delta x \sim 0.1$) for reduced frequencies above 0.1 and less than approximately 3. The acoustic responses for high aspect ratio wings were found to agree well qualitatively with the 2D results. As an illustration of the capabilities of the method, a full-span, flapped wing configuration undergoing oscillatory motion was considered with a preliminary quantification of the aeroacoustic influence of the flap.

NOMENCLATURE

a	speed of sound
A	gust amplitude
AR	aspect ratio
b, c	span, chord length
C_l, C_L	2D, 3D lift coefficient
C_P	coefficient of pressure
$\frac{D_\infty}{Dt} = \frac{\partial}{\partial t} + U_\infty \frac{\partial}{\partial x_1}$	linearized material derivative
$\frac{D_w}{Dt} = \frac{\partial}{\partial t} + \mathbf{v}_w \cdot \nabla$	wake convective derivative
f	frequency of oscillation
l, L	2D, 3D lift force
M	Mach number
N_1, N_2	number of streamwise, spanwise panels
G	Green's function
$H(x)$	Heaviside step function
U_∞	undisturbed freestream velocity
$\mathbf{n}$	outward unit normal vector
$\mathbf{r}$	radial vector (source to observer)
$(\mathbf{x}, t), (\mathbf{y}, \tau)$	source, observer position and time
$\mathbf{v}_w = \frac{(\mathbf{v}_+ + \mathbf{v}_-)}{2}$	wake convective velocity
β	Prandtl-Glauert parameter
δ	flap deflection angle
$\theta = \cos^{-1}(\mathbf{n} \cdot \frac{\mathbf{r}}{r})$	observer declination angle
$\rho, \mathbf{v}, p$	fluid density, velocity, and pressure
ϕ	perturbation velocity potential
$\omega = (2\pi f)c/2U_\infty$	reduced frequency of oscillation

Subscripts:

i	i^{th} spatial coordinate

Superscripts:

(B)	solid body part
(W)	wake part
$+, -$	above, below ($\pm\mathbf{n}$) wake

Overscripts:

$\tilde{}$	Prandtl-Glauert space
$\dot{}$	time derivative

*Student Member ASME
†Member ASME

INTRODUCTION

The reduction of aircraft noise is an important consideration for current and future aircraft designs as environmental noise pollution becomes increasingly detrimental with increased air traffic. The predominant sources of aircraft noise include jet noise, airframe noise from high-lift systems and landing gear, and blade-vortex interaction (BVI) noise from helicopter rotors. This noise is generated by unsteady flow fluctuations (from vorticity or turbulence) and their interaction with solid surfaces nearby. Although jet noise tends to dominate at take-off, airframe noise has been observed to dominate over jet noise in certain landing situations (Michel et al. 1998). The goal of the current research is to develop efficient tools for the investigation of airframe noise.

There is currently a need to bridge the gap between highly idealized analytical solutions and computationally intensive numerical simulations. For most flows of practical interest, numerical solutions are necessarily three-dimensional and require a full 3D-grid to perform a RANS or LES simulation. To apply such techniques to highly-complicated geometries and to obtain acoustic information forces their application to the late stages of design or for highly reduced parametric studies because of the high computational complexity involved. In the present research, a balance between robustness and physical modelling is sought. By modelling only the dominant flow features effectively, a more efficient aeroacoustic prediction tool may be obtained while retaining the ability to analyze geometrically complex systems.

It is believed that many of the dominant acoustic generation mechanisms for high-lift wing systems can be modelled well (Guo 1997) within the framework of Boundary Element Methods (BEM). Researchers have previously used BEM techniques in 2D and 3D to study helicopter rotor and turbomachinery noise (Lee et al. 1990; Yao & Liu 1998; Gennaretti et al. 1997), both of which involve sound generation mechanisms similar to those found in airframe noise (e.g., wakes from upstream structures convecting past downstream structures). This paper briefly describes the adaptation of the BEM work of Morino et al. (1975) for airframe noise. The solution is calculated in the time domain and allows for a free-wake evolution. Of interest for airframe noise is the application of this method to multielement, fixed wing configurations to calculate the unsteady near-field forces and the acoustic pressure in the field surrounding the wing.

In this method, the assumptions that the flow Reynolds number is high and remains attached allow one to model the boundary layers and wakes by surface source distributions (i.e., source and doublet/vortex layers). Wakes are generated at sharp trailing edges in the wing geometry and can be evolved freely under the influence of the surrounding fluid. The current paper follows the work of (Wood & Grace 2000) where an incompressible implementation of the present BEM with a free-wake analysis was applied to a wing-flap configuration. The present work extends the implementation to include the effect of subsonic compressibility. As this methodology develops, it is critical to validate the numerical results with classical solutions (although the authors have yet to find other similar validations for 3D compressible, time-domain, BEM computations in the literature). This paper shows the comparison between postprocessed time-domain results from the current method and canonical 2D, frequency-domain solutions for a thin, flat-plate airfoil in a transverse gust (Atassi et al. 1993). In addition to the validation, the paper also presents preliminary results showing the effect of a full-span flap on both the wake development and the acoustic field produced by an oscillating wing.

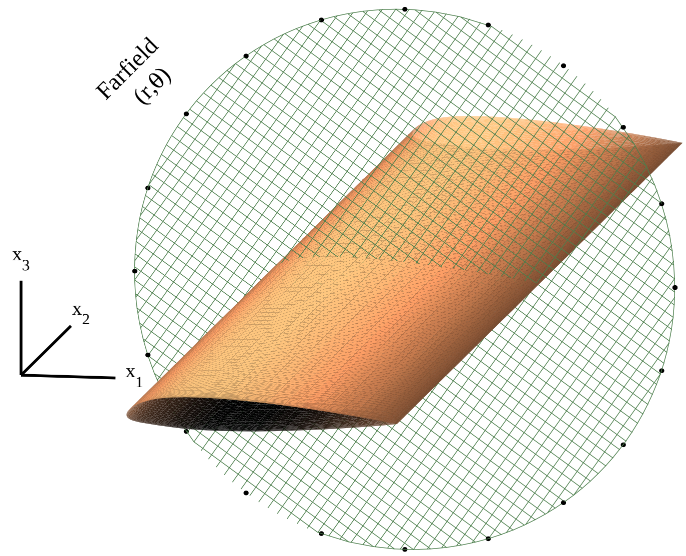

Figure 1. Problem schematic

METHOD

Consider fully-attached, high Reynolds number flow around a rectangular wing as shown in Figure 1. The present research uses the Boundary Element Method (BEM) as formulated for quasi-potential flows (Morino et al. 1975; Gennaretti et al. 1997). The flow is modelled to be potential everywhere off the solid wing surfaces and outside the wakes. Fully attached, high Reynold's number flows are assumed such that viscous effects are prevalent only in the wake generation at the trailing edges of the wing elements. The flow velocity infinitely far from the wing is taken to be uniform in the x_1 direction and to be in the low subsonic regime.

Governing Equations: Under the above assumptions, the perturbation velocity potential is known to satisfy the convective wave equation (Morino 1993)

$$M^2 \frac{D_\infty^2 \phi}{Dt^2} - \nabla^2 \phi = 0, \tag{1}$$

where space and time have been scaled by the half-chord length $c/2$ and the convective time scale $c/2U_\infty$, respectively. The solution to Eq. (1) satisfies the boundary integral equation

$$-\frac{1}{4\pi} \int_{\tilde{S}} \left[\frac{1}{\tilde{r}} \frac{\partial \tilde{\phi}(\tilde{\mathbf{y}}, \tau)}{\partial \tilde{n}} + \frac{\tilde{\mathbf{r}} \cdot \tilde{\mathbf{n}}}{\tilde{r}^2} \left(\frac{\tilde{\phi}}{\tilde{r}} + \frac{\dot{\tilde{\phi}}}{\tilde{a}} \right) \right]^{\tau^\star} d\tilde{\mathbf{y}}$$

$$= \begin{cases} \tilde{\phi}(\tilde{\mathbf{x}}, \tilde{t}) & \text{, for } \mathbf{x} \text{ in field} \\ \frac{1}{2} \tilde{\phi}(\tilde{\mathbf{x}}, \tilde{t}) & \text{, for } \mathbf{x} \text{ on wing} \\ 0 & \text{, for } \mathbf{x} \text{ inside wing} \end{cases} \tag{2}$$

where $\tau^\star = \tilde{t} - \tilde{r}/\tilde{a}$, $\tilde{a} = \beta/M$, $\tilde{r} = |\tilde{\mathbf{x}} - \tilde{\mathbf{y}}|$, and tildes denote evaluation in the Prandtl-Glauert space—

$$(\tilde{\mathbf{x}}, \tilde{t}) = \left(\frac{x_1}{\beta}, x_2, x_3, t - \frac{M^2 x_1}{\beta^2} \right). \tag{3}$$

Equation (2) is solved numerically by applying a zeroth-order Boundary Element Method and linear time interpolation to give a set of algebraic equations (Morino 1980)

$$H\phi_i^n = \sum_j G_{D_{ij}}^{(B)} \phi_j^{n-\tau_{ij}} - G_{S_{ij}}^{(B)} \mathrm{v}_{n_j}^{n-\tau_{ij}} + G_{R_{ij}}^{(B)} \dot{\phi}_j^{n-\tau_{ij}} +$$
$$G_{D_{ij}}^{(W)} \Delta\phi_j^{n-\tau_{ij}} + G_{R_{ij}}^{(W)} \Delta\dot{\phi}_j^{n-\tau_{ij}}, \tag{4}$$

where,

$$\tau_{ij} = \frac{M}{\beta} \left(r_{\beta_{ij}} + M r_{1_{ij}} \right), \tag{5}$$

$$r_{\beta_{ij}} = \sqrt{(x_{i_1} - y_{j_1})^2/\beta^2 + (x_{i_2} - y_{j_2})^2 + (x_{i_3} - y_{j_3})^2}. \tag{6}$$

The indices i, j, and n refer to the collocation point, panel index, and time iteration, respectively. The wing body and wake surface are denoted by (B) and (W), and G_S, G_D, and G_R refer to the source, doublet and ratelet influence matrices.

By applying equations (4) to collocation points located at the center of each panel on the body, a time-domain solution for the surface distributions of ϕ is readily obtained. The flow velocity and pressure may then be determined through differentiation and Bernoulli's equation. Once the aerodynamic solution is calculated, the acoustic field may be evaluated directly using the computed aerodynamic sources with newly computed influence matrices for observer points in the surrounding fluid. This formulation provides an inherent consistency ideally suited for aeroacoustic studies.

Boundary Conditions: The solid surfaces of the wing are impermeable. Thus, the normal perturbation velocity is required to satisfy

$$\mathbf{U}_\infty \cdot \mathbf{n} + \frac{\partial \phi}{\partial n} = 0. \tag{7}$$

The wakes are modelled as infinitely thin shear layers and, therefore, cannot support a pressure jump. By applying Bernoulli's equation to a point $\mathbf{x}_+$ just above and $\mathbf{x}_-$ just below the wake, one obtains

$$\frac{\partial \Delta\phi}{\partial t} + \frac{1}{2}(\mathrm{v}_+^2 - \mathrm{v}_-^2) = \frac{\partial \Delta\phi}{\partial t} + \frac{(\mathbf{v}_+ + \mathbf{v}_-)}{2} \cdot (\mathbf{v}_+ - \mathbf{v}_-) =$$
$$\frac{D_w}{Dt}(\Delta\phi) = 0, \tag{8}$$

where

$$\frac{D_w}{Dt} = \frac{\partial}{\partial t} + \mathbf{v}_w \cdot \nabla = \frac{\partial}{\partial t} + \frac{(\mathbf{v}_+ + \mathbf{v}_-)}{2} \cdot \nabla. \tag{9}$$

Equation (8) is the condition which relates the wake strength $\Delta\phi$ to the potential jump at the trailing edge when the wake element was located at that trailing edge. Additionally, the wake evolution is determined such that the fluid elements in the wake are convected with the average velocity across the sheet. This defines a *free-wake* evolution which is described in greater detail in Ramsey (1996) and Wood & Grace (2000).

Numerical Model and Grid Convergence: For purposes of numerical validation, a very thin wing at zero angle of attack to the freestream experiencing a small amplitude oscillatory gust is considered. The gust is chosen to correspond to the Sears problem (Sears 1941) such that the boundary condition Eq. (7) may be written

$$\frac{\partial \phi}{\partial n} = -n_1 U_\infty - n_2 A \sin[w(t - x_{\mathrm{mc}})], \tag{10}$$

where x_{mc} denotes the x_1 position of the midchord and A is the gust amplitude. Note that in the limit of zero wing thickness, the mean flow does not influence the solution when the wing is at zero degrees angle of attack.

In Figure 2a, the lift coefficient is presented for a wing with an aspect ratio $AR = 10$, a gust with a reduced frequency of $\omega = 0.4$, and a Mach number of $M = 0$. Three different grid resolutions are presented to show convergence. Because the zeroth order BEM exhibits a first-order convergence, an estimate of the

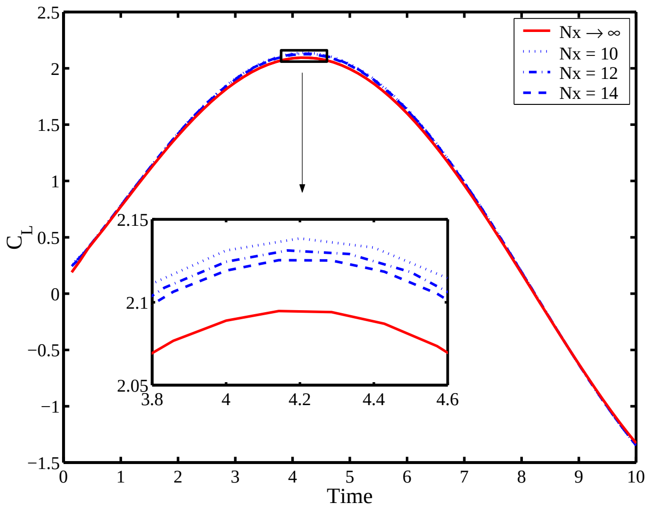

a) Time-domain solution

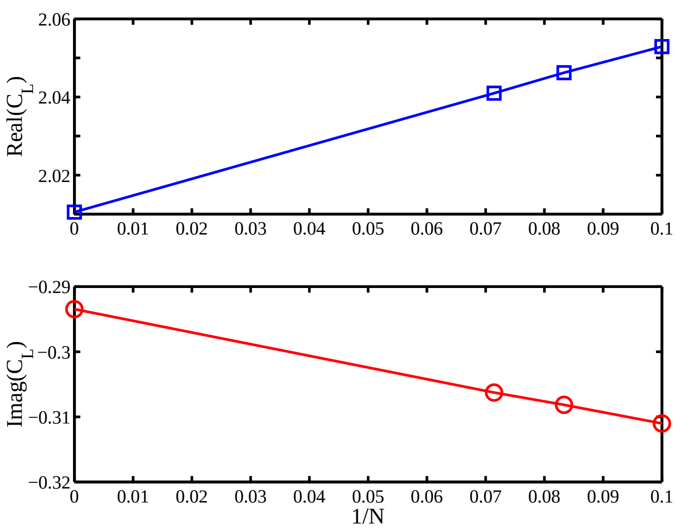

b) Frequency domain data

Figure 2. Grid convergence

"converged" solution may be obtained by finding the y-intercept of a straight line passing through the data plotted against $1/N_1$ (Moran 1984), where N_1 is the number of elements in the streamwise direction. Performing this extrapolation for each timestep yields the solid curve in Figure 2a.

This linear extrapolation is illustrated in Figure 2b where the complex amplitude is determined for all three discretizations in Figure 2a at the gust frequency and plotted versus $1/N_1$. All other grid parameters such as the spanwise panel length $1/N_2$, the timestep Δt, the wing thickness, etc., should be chosen so as to decrease proportionally as $1/N_1$ is decreased. This gives convergence along the diagonal in the parameter space because of the linear convergence of the method.

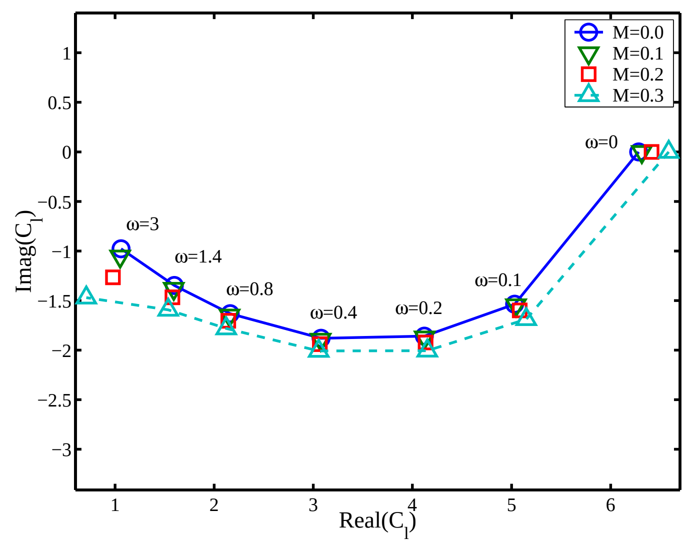

Figure 3. 2D lift amplitude

2-D COMPARISONS

The near-field and far-field responses of a 2D flat-plate airfoil to a transverse gust are calculated here following the method of Atassi, Dusey, & Davis (1993). In Figure 3, the complex lift coefficient is modified by a factor $\exp(-i\omega)$ to simplify the response given by the well-known Sears function (Sears 1941).[1] The circles denote the analytical solution for $M = 0$ given by Sears whereas the $M = 0.1, 0.2, 0.3$ results were obtained from the semi-analytic solution of Atassi, Dusey, & Davis (1993). The 2D lift coefficient is defined by

$$C_l = \frac{l}{\rho U_\infty A \frac{c}{2}} \tag{11}$$

The far-field complex pressure amplitudes were also calculated by Atassi et al. (1993) and are presented in Figure 4 for four cases: $M = 0.1, 0.3$ and $\omega = 0.1, 0.8$. In each plot, the dashed and solid lines refer to the real and imaginary parts, respectively. The far-field observer locations are positioned on a circle surrounding the airfoil and centered on the midchord (see Fig. 1). The azimuthal coordinate is taken positive counterclockwise from the

[1] This modification is equivalent to referencing the gust to the leading edge of the airfoil as opposed to the midchord (Giesing, Rodden, & Stahl 1970).

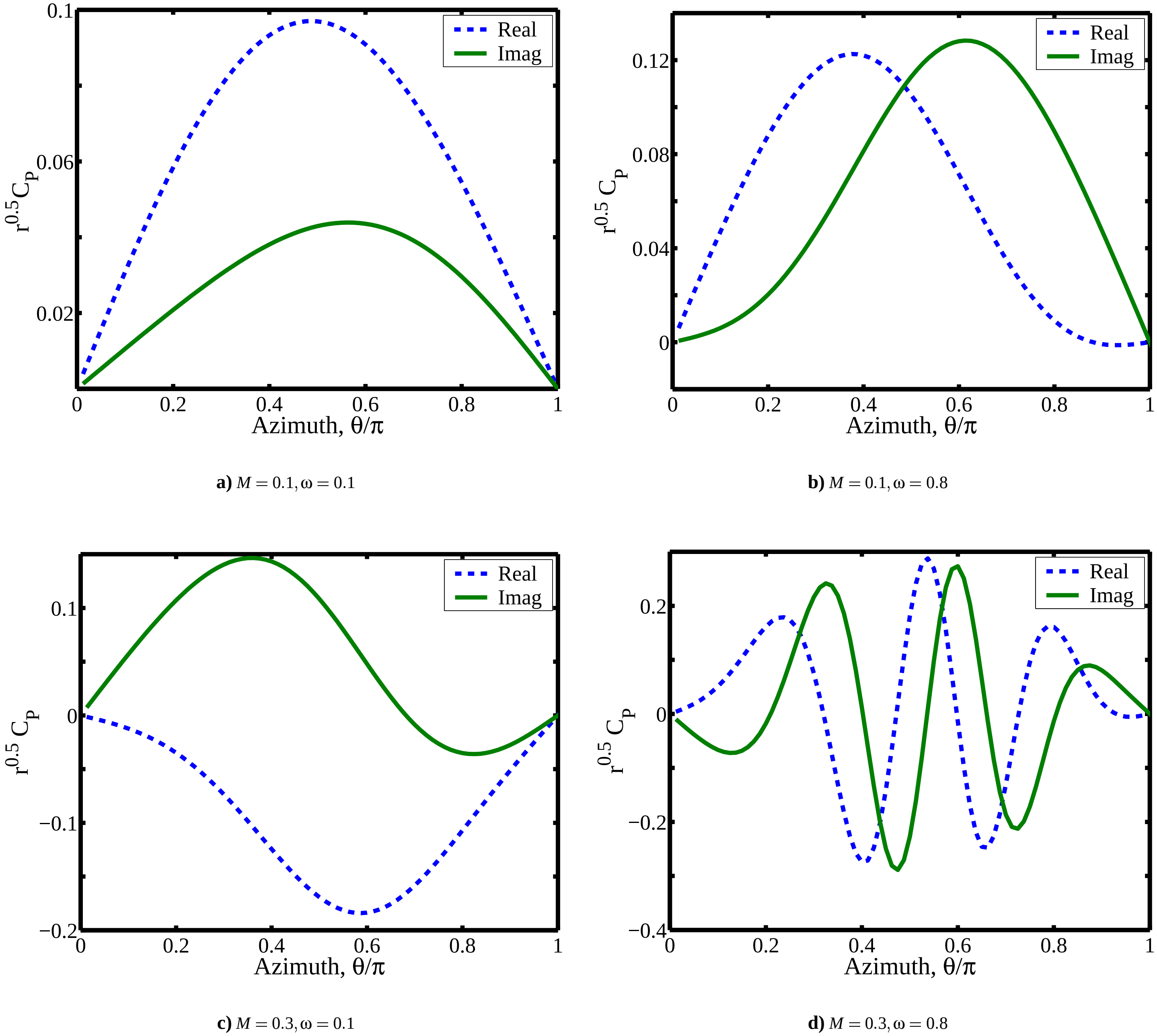

a) $M = 0.1, \omega = 0.1$

b) $M = 0.1, \omega = 0.8$

c) $M = 0.3, \omega = 0.1$

d) $M = 0.3, \omega = 0.8$

Figure 4. 2D far-field pressure

$+x_1$ axis. The radius of the observer circle was taken to be 100 half-chords.

3-D RESULTS

Calculations using the 3D compressible time-domain BEM were performed to be compared to well-established 2D solutions for thin, flat-plate airfoils. To attain the desired correspondence, a rectangular wing with a parabolic profile was used. The wing thickness was chosen so as to decrease proportionately with $1/N_1$ using a 10%-chord thickness for the $N_1 = 10$ grid. A flat-wake model ($\mathbf{v}_w = [\mathbf{v}_+ + \mathbf{v}_-]/2 = U_\infty \hat{i}$) was also used so as to match the 2D analytical model.

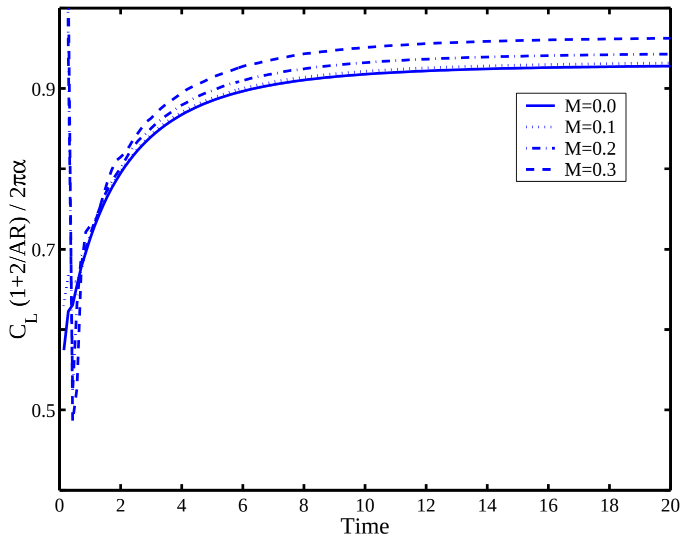

Figure 5. Response to impulsively-started flow

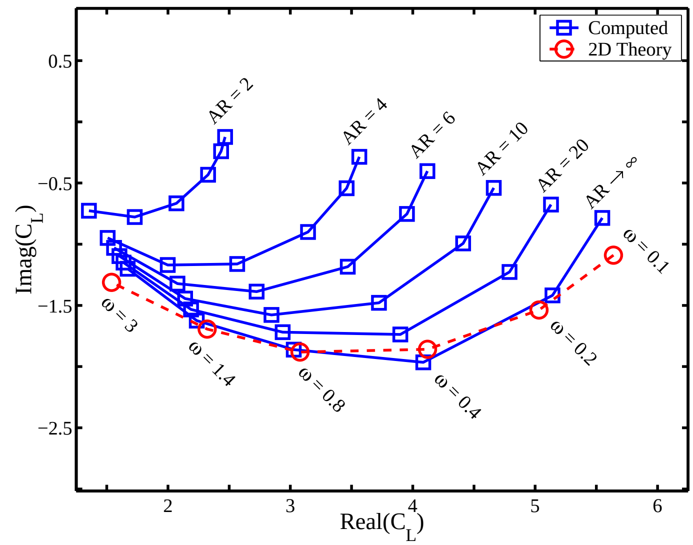

Figure 6. Effect of Aspect Ratio

Aerodynamics

The response of a thin rectangular wing ($AR = 10$) subjected to impulsively started flow at one degree angle of attack is presented in Figure 5. Results for Mach numbers between 0 and 0.3 are presented and were obtained using the extrapolated convergence method outlined in the method section. The 3D lift coefficient is defined as

$$C_L = \frac{L}{\frac{1}{2}\rho U^2 cb}, \tag{12}$$

where b is the span length. Note the appearance of a delta function at $t = 0$ arising because of the step jump in the potential.[2] The Mach number is seen to increase the lift as well as the strength of the initial impulse.

The incompressible Sears gust response is presented for rectangular wings of varying aspect ratio in Figure 6. The Sears solution is given by the circles and dashed curve whereas the 3D results are given by the squares and solid curves. The 3D lift coefficient is defined by

$$C_L = \frac{L}{\rho U A \frac{bc}{2}}, \tag{13}$$

Each gust frequency is calculated by performing the extrapolated convergence method on all of the frequency domain data obtained from each time domain calculation. In addition, aspect ratios of 2, 4, 6, 10, and 20 were calculated and an estimate for $AR \to \infty$ was obtained by extrapolating for $1/AR \to 0$. A good correspondence is observed except for the highest and lowest frequencies. The high frequencies will fail when the grids using $N = 10, 12,$ and 14 are too coarse to resolve the temporal variation. For these cases, calculations for higher N are required. The low frequencies incur error because the time-domain solution is not carried on indefinitely. For these cases, the simulation time must be extended beyond 20 units of time. The results using $N = 10, 12,$ and 14 are seen to be accurate to less than 5% for frequencies higher than 0.1 and less than approximately 3.

The effect of the Mach number on the gust response for an $AR = 20$ wing is shown in Figure 7. The solid and dashed curves denote the $M = 0$ and $M = 0.3$ cases respectively. When comparing Figure 7 to Figure 3, note that the differences are due primarily to the low and high frequency errors discussed above, and to the effects of the finite aspect ratio.

Acoustic Radiation

The far-field acoustic pressure was calculated using the aerodynamic solutions presented above. The observer locations are a distance of 200 half-chords from the center of the wing and situated on a circle centered around the centerspan of the wing as illustrated in Figure 1. The four cases for $M = 0.1, 0.3$ and $\omega = 0.1, 0.8$ ($AR = 20$) are shown as in Fig. 4. The comparison between the 2D calculations is qualitatively good. Differences do exist, however, because of both discretization errors and the fundamental differences in 2D versus 3D acoustic propagation. The coefficient of pressure scales with $\sqrt{r}$ and r in 2D and 3D, re-

[2] The time derivative of the potential appears in Bernoulli's equation for the pressure:

$$C_p = \frac{p - p_\infty}{\frac{1}{2}\rho U_\infty^2} = 1 - v^2 - 2\dot{\phi}$$

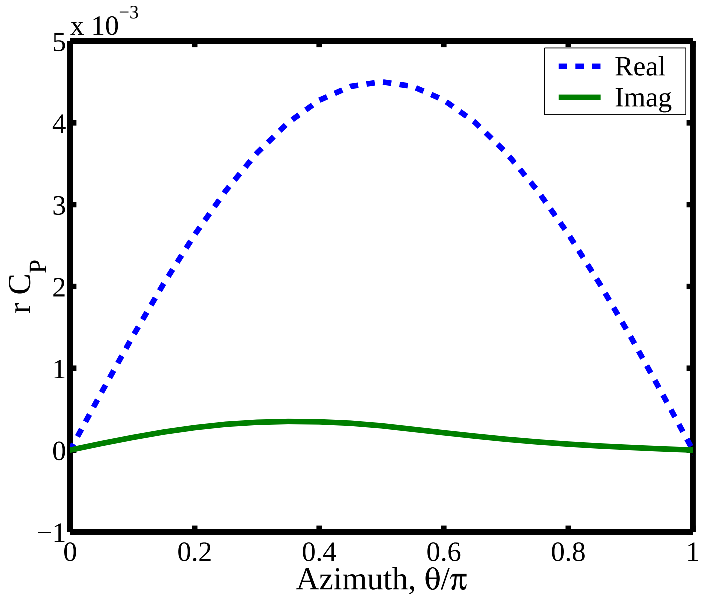

a) $M = 0.1, \omega = 0.1$

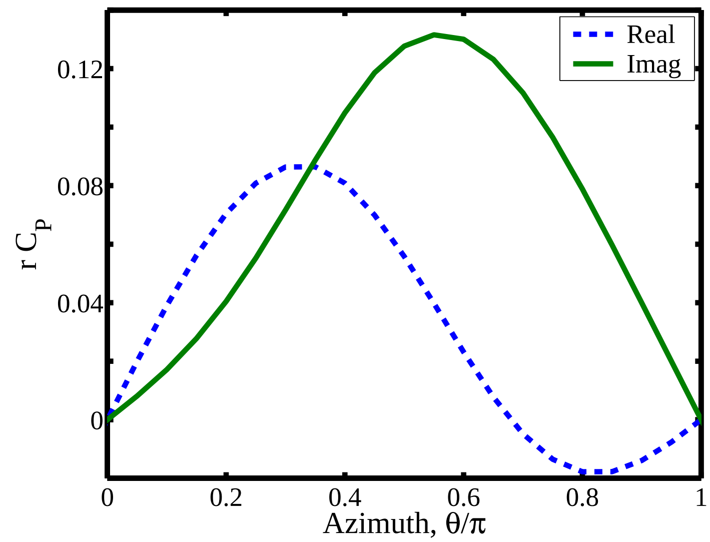

b) $M = 0.1, \omega = 0.8$

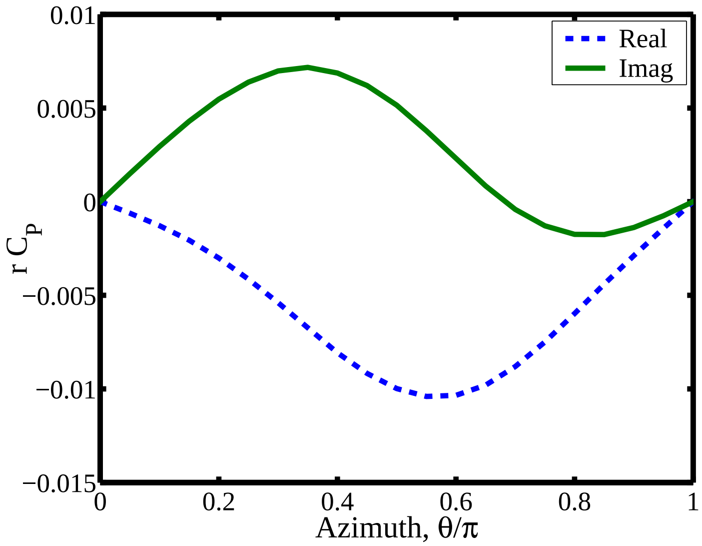

c) $M = 0.3, \omega = 0.1$

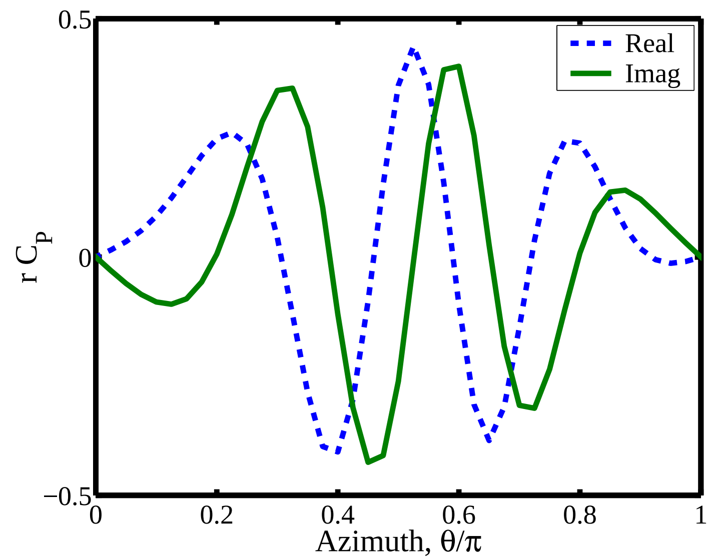

d) $M = 0.3, \omega = 0.8$

Figure 8. 3D far-field pressure

spectively; however, a dependence on M and ω is also expected. In comparing the maximum C_p depicted in figures 4 and 8, one finds a reasonably close correspondence at $\omega = 0.8$ while the 3D results at $\omega = 0.1$ fall short of the corresponding 2D results by a factor of about 20. This may be correlated perhaps to the results in Figure 6 where the lift coefficient is more significantly affected by the aspect ratio at low frequencies than at higher frequencies. In addition, the far-field asymptotic behaviour of the 2D Greens function for the Helmholtz equation $H_0^{(2)}(Kr)$ scales with $\sqrt{K} = \sqrt{M\omega}/\beta$ which gives $\sqrt{K} = 0.1, 0.29, 0.19,$ and 0.54

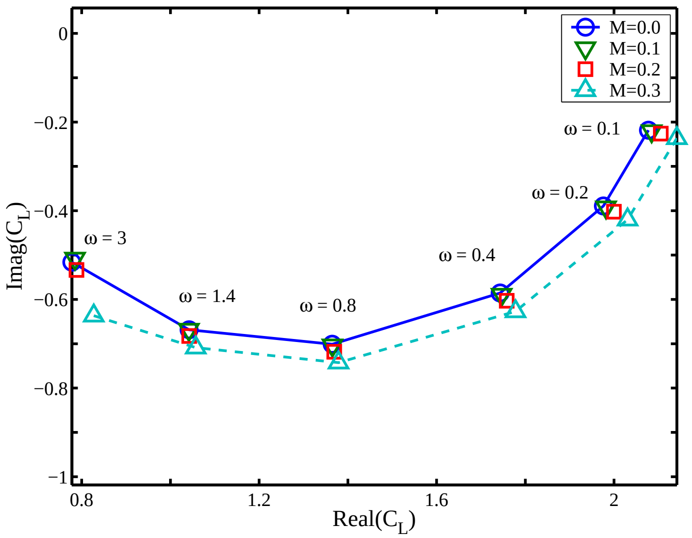

Figure 7. Effect of Mach Number

for cases (a) through (d) in Figure 4.

Flapped Wing

The objective of the present work was to validate a 3D compressible time-domain BEM with 2D analytical solutions for an ideally flat wing. The ultimate purpose, however, is to apply this method to more practical systems. As a preliminary illustration, the flow around a NACA 23012 wing in heave oscillation and with a NACA 6412 flap at 20 degrees deflection is presented here. Consider a heave amplitude that is 10% of the freestream velocity such that the boundary condition Eq. (7) may be written

$$\frac{\partial\phi}{\partial n} = -n_1 - n_2\,(0.1)sin(\omega t). \tag{14}$$

An incompressible ($M = 0$) calculation for $\omega = 2$ ($f = 1/\pi$)) was performed using a free-wake analysis ($\mathbf{v}_w$ calculated explicitly). Resulting wake configurations are presented without and with the flap in figures 9 and 10. The wake is seen to distort more significantly with the flap present. In Figure 9b, the grid is seen to be too coarse to fully resolve the tip and starting vortices.

The frequency spectrum (FFT) of the pressure coefficient is shown in Figure 11 for a far-field observer located at $r = 100$ and $\theta = -\pi/2$. The signal energy is seen to be increased with the presence of the flap.

Future Work

The example presented above helps to highlight issues for future consideration. Currently, the compressibility effects are accounted for via the Prandtl-Glauert transformation for steady, translational motion. The general influence for a freely-evolving wake involves the solution of a transcendental equation for the retardation time. How much will this affect the far-field evaluation and the free-wake evolution itself?

The method will also be used to investigate the aeroacoustic response to the passing of a free vortex. The results may be compared to the analytical theory of Howe (1999).

CONCLUSIONS

The validation of a 3D time-domain, compressible Boundary Element Method for subsonic flow around a thin rectangular wing has been performed. The aeroacoustic response of the wing in a sinusoidal transverse gust was obtained and compared to 2D analytical theory. An extrapolation method was used to estimate the converged numerical solution using three different grid refinements for each calculation of interest. It was found that frequency-domain lift solutions accurate to less than 5% can be readily obtained using relatively coarse grids for reduced frequencies above 0.1 and less than approximately 3. By increasing the resolution of the grids and lengthening the extent of the simulation time, accuracy may be improved for the higher and lower frequencies, respectively. The aerodynamic solutions obtained using this convergence method were used to calculate acoustic signals in the far field. These acoustic calculations for high aspect ratio wings were found to agree well qualitatively with the 2D results.

In addition to the validation, the application of the method to compute the aeroacoustic response of a full-span, flapped wing configuration undergoing oscillatory motion was presented. This preliminary result exemplifies the capability of the method for computing the sound produced from flow past complex structures in three dimensions.

ACKNOWLEDGMENT

The authors would like to thank Luigi Morino for the invaluable help throughout the duration of this work, as well as Kadin Tseng, Yueping Guo, and Rahul Sen for the helpful discussions. This research has been supported by the National Sciences and Engineering Research Council of Canada and the Boeing Company.

REFERENCES

Atassi, H. M., Dusey, M., & Davis, C. M. 1993, “Acoustic Radiation from a Thin Airfoil in Nonuniform Subsonic Flow,”*AIAA Journal*, Vol. 31, 12–19.

Gennaretti, M., Luceri, L., & Morino, L. 1997, “A Unified Boundary Integral Methodology for Aerodynamics and Aeroacoustics of Rotors,”*J. Sound and Vib.*, Vol. 200, 467–89.

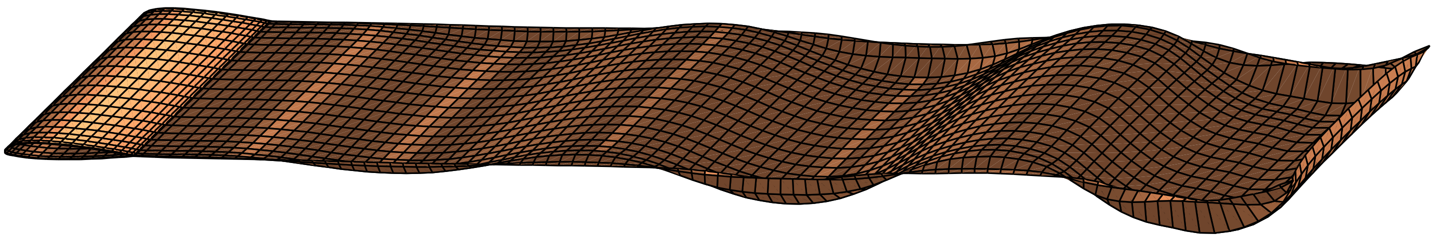

a) NACA 23012 without flap

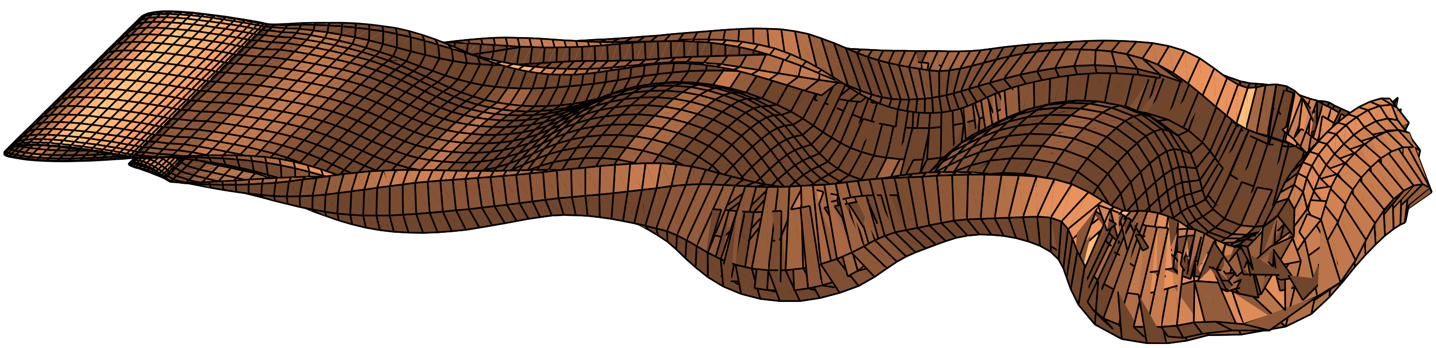

b) with NACA 6412 flap

Figure 9. 3D wake shapes

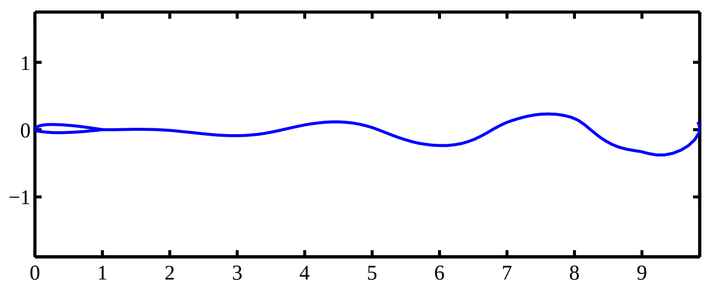

a) without flap

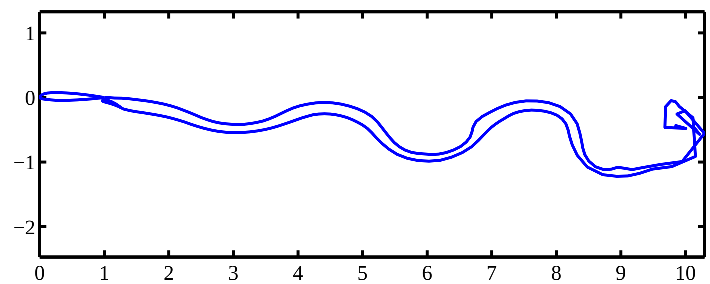

b) with flap

Figure 10. Centerspan section of wake shapes

Giesing, J. P., Rodden, W. P., & Stahl, B. 1970, "Sears Function and Lifting Surface Theory for Harmonic Gust Fields,"*Journal of Aircraft*, Vol. 7, 252–255.

Guo, Y. P. 1997, "A Model for Slat-Noise Generation,". In *Proceedings of the 3rd AIAA/CEAS Aeroacoustics Conference*, Atlanta, GA. Paper no. AIAA-97-1647.

Howe, M. S. 1999, "Trailing Edge Noise at Low Mach Numbers,"*J. Sound Vib.*, Vol. 255, 211–238.

Lee, Y. T., Jiang, C. W., & Bein, T. W. 1990, "Rotor/Stator Flow Coupling in Turbomachines,". In *Proc. of 3rd Intern. Sym. on Transport Phenomena and Dynamics of Rotating Machinery*.

Michel, U., Barsikow, B., Helbig, J., Hellmig, M., & M. Schüttpelz 1998, "Flyover Noise Measurements on Landing Aircraft with a Microphone Array,". In *Proceedings of the 4th AIAA/CEAS Aeroacoustics Conference*, Toulouse, France. Paper no. AIAA-98-2336.

Moran, J. 1984, *An Introduction to Theoretical and Computational Aerodynamics*. Wiley.

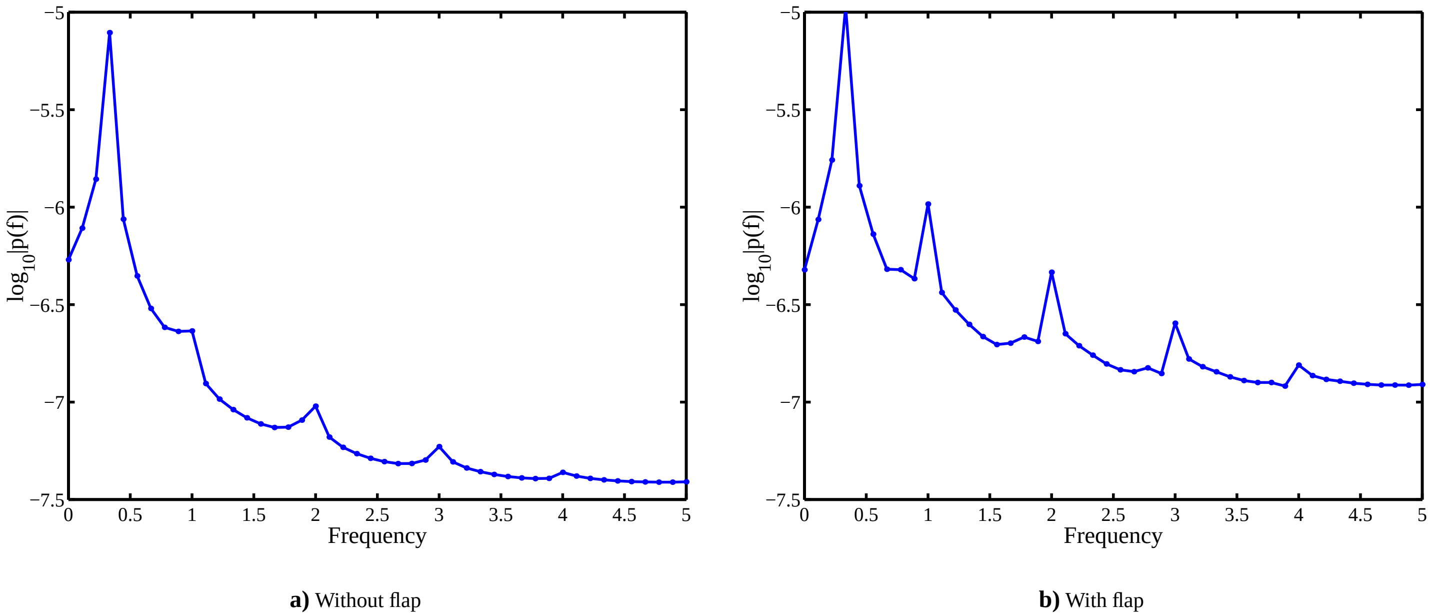

Figure 11. Computed spectra of far-field pressure coefficient at flyover

Morino, L. 1980, "Steady, Oscilatory, and Unsteady Subsonic and Supersonic Aerodynamics — Production Version (SOUSSA-P1.1) Vol. 1, Theoretical Manual,". Technical Report CR-159130, NASA.

Morino, L. 1993, "Boundary Integral Equations In Aerodynamics,"*Appl. Mech. Rev.*, Vol. 46, 445–66.

Morino, L., Chen, L.-T., & Suciu, E. 1975, "Steady and Oscillatory Subsonic and Supersonic Aerodynamics around Complex Configurations,"*AIAA J.*, Vol. 13, 368–374.

Ramsey, W. D. 1996, *Boundary integral methods for Lifting Bodies with Vortex Wakes*. Doctoral dissertation, Massachusetts Institute of Technology, Cambridge, Massachusetts.

Sears, W. R. 1941, "Some Aspects of Non-Stationary Airfoil Theory and Its Practical Application,"*Journal of the Aeronautical Sciences*, Vol. 8, 104–108.

Wood, T. H. & Grace, S. M. 2000, "Free-Wake Analysis for Calculating the Aeroacoustics of a Wing-Flap Configuration,". In *Proceedings of the 38th AIAA Aerospace Sciences Meeting*, Reno, NV, 162–173. Paper no. AIAA 2000-0607.

Yao, Z. X. & Liu, D. D. 1998, "Vortex Dynamics of Blade-Blade Interaction,"*AIAA J.*, Vol. 36, 497–504.